Optimizing snake locomotion on an inclined plane

Xiaolin Wang,[1,2,*] Matthew T. Osborne,[1,3] and Silas Alben[1,†]
[1]*Department of Mathematics, University of Michigan, Ann Arbor, MI 48109, USA*
[2]*School of Mathematics, Georgia Institute of Technology, Atlanta, Georgia 30332, USA*
[3]*Department of Mathematics and Statistics, University of Toledo, Toledo, Ohio 43606, USA*
(Received 18 October 2013; published xxxxxx)

We develop a model to study the locomotion of snakes on inclined planes. We determine numerically which snake motions are optimal for two retrograde traveling-wave body shapes, triangular and sinusoidal waves, across a wide range of frictional parameters and incline angles. In the regime of large transverse friction coefficients, we find power-law scalings for the optimal wave amplitudes and corresponding costs of locomotion. We give an asymptotic analysis to show that the optimal snake motions are traveling waves with amplitudes given by the same scaling laws found in the numerics.

DOI: 10.1103/PhysRevE.00.002700 PACS number(s): 87.19.ru, 87.19.rs, 87.10.Ca, 45.40.Ln

I. INTRODUCTION

Snake locomotion has long drawn the interest of biologists, engineers, and applied mathematicians [1–5]. A lack of limbs distinguishes snake kinematics from other common modes of locomotion such as swimming, flying, and walking [6]. Snakes propel themselves by a variety of gaits, including slithering, sidewinding, concertina motion, and rectilinear progression [4]. They can move in terrestrial [1,7], aquatic [8], and aerial [9] environments. Snake-like robots have shown impressive locomotor abilities [2,10,11], with applications in confined environments like narrow crevices [12], as well as rough terrain [13]. In such environments the ability to ascend an incline is fundamental, and various studies of snakes and snake-like robots have been conducted on this subject. Maneewarn and Maneechai [5] examined the kinematics of crawling gaits in narrow inclined pipes with jointed modular snake robots and found that high speeds were obtained with short-wavelength motions. Hatton and Choset [14] focused on sidewinding gaits on inclines and presented stability conditions for snakes by comparing sidewinding to a rolling elliptical trajectory and determining the minimum aspect ratio of the sidewinding pattern to maintain stability. Marvi and Hu [15] studied concertina locomotion on steep slopes and in vertical crevices. They found that snakes can actively orient their scales and lift portions of their bodies to vary their frictional interactions with the surroundings. Transeth *et al.* [16] considered the obstacle-aided locomotion of snake robots on inclined and vertical planes. They found agreement with a numerical model that included both frictional forces and forces from rigid-body contacts with the obstacles.

A common way to study locomotory kinematics is to propose a form of efficiency and determine the kinematics which optimize it. Some well-known examples include locomotor studies of organisms in low- [17–20] and high-Reynolds-number fluids [21–23]. In this work, we apply the same methodology and focus on the undulatory motions of snakes on an inclined plane by extending a recently proposed model for motions on a horizontal plane [4,24–26] to those on an incline. Here the snake is a slender body whose curvature is prescribed as a function of arc length and time. For simplicity, we do not consider elasticity or viscoelasticity in the snake body. The external forces acting on the snake body are Coulomb friction with the ground and gravity. The model has shown good agreement with biological snakes on a horizontal plane [4,24], and previous studies have used the model to find optimally efficient snake motions. Hu and Shelley [24] prescribed a sinusoidal traveling-wave body motion and found the optimally efficient amplitude and wavelength of the traveling wave. Jing and Alben [25] used the same model to consider the locomotion of two- and three-link snakes. They found optimal motions analytically and numerically in terms of the temporal functions for the internal angles between the links. Alben [26] considered more general snake shapes and motions by prescribing the curvature as a function of arc length and time with 45 (and 180) parameters and optimizing it across the space of frictional coefficients. He found that the optimal motions are retrograde and direct traveling-wave motions for large and small transverse friction coefficients, respectively. In the large transverse friction coefficient regime, he showed analytically that the optimal motion is a traveling wave and found the scaling laws for the wave amplitude and cost of locomotion with respect to the friction coefficients, both numerically and analytically.

In this paper, we confine our discussion to the regime where the transverse friction coefficient is larger than the tangential friction coefficients. This is the typical regime for biological and robotic snakes [2,24]. We prescribe the snake's motion as a retrograde traveling wave with two shape profiles, triangular and sinusoidal, but with undetermined amplitudes. The triangular wave motion has analytical solutions and embodies many aspects of general traveling-wave motions. We obtain the optimal motions in terms of the amplitude of the triangular wave in the three-parameter space spanned by transverse frictional coefficients, tangential (forward) frictional coefficients, and incline angles. We discuss the relative effects of these three parameters and find the upper bound of the incline angle for the snake to maintain an upward motion. We also find the power-law scalings for the optimal amplitudes and corresponding costs of locomotion with respect to the three parameters. For the sinusoidal wave motion, we use a numerical method to solve for the position of the snake body

*xiaolinw@gatech.edu
†alben@umich.edu

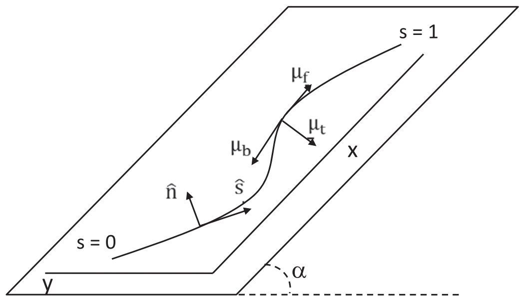

FIG. 1. Schematic of the snake position on a plane inclined at angle α. The arc length s is nondimensionalized by the snake length. The tangent and normal vectors are labeled at a point. Forward, backward, and transverse velocity vectors are shown with corresponding friction coefficients μ_f, μ_b, and μ_t.

from its prescribed curvature. We then obtain the optimal body shape numerically and show that it follows the same scaling laws as the triangular wave motion, providing confirmation of those results. In the last part of the paper, we analytically determine the asymptotic optima for more general snake motions in the regime of a large transverse friction coefficient. We obtain the same scalings analytically as those found for the triangular and sinusoidal waves, which confirms and generalizes those results. Our study of snake locomotion can also be generalized to other locomotor systems as long as the same frictional law applies. One example is the undulatory swimming of sandfish lizards in sand [27,28].

This paper is organized as follows: Sec. II describes the mathematical model for snake locomotion on an inclined plane. Section III studies the optima of the triangular wave motion, and Sec. IV studies those of the sinusoidal wave motion. The analytical asymptotic calculation is presented in Sec. V, and the conclusions follow in Sec. VI.

II. MODEL

We use the same frictional snake model as [4,24–26] to describe snake locomotion on an incline. The snake body is a curvilinear segment given by $\mathbf{X}(s,t) = (x(s,t), y(s,t))$, a function of arc length s and time t. The unit vectors tangent and normal to the snake body are $\hat{\mathbf{s}}$ and $\hat{\mathbf{n}}$, respectively. The snake is placed on a plane inclined at angle α with respect to the horizontal plane. The x-y axes are oriented with the $+x$ axis extending from the origin directly up the incline, and the $+y$ axis is rotated 90° from it and directed across the incline. Height is constant along the y axis. A schematic diagram is shown in Fig. 1.

The tangent angle and the curvature are denoted $\theta(s,t)$ and $\kappa(s,t)$. Given the curvature, the tangent angle and the position of the snake body can be obtained by integrating

$$\theta(s,t) = \theta_0(t) + \int_0^s \kappa(s',t)\,ds', \tag{1}$$

$$x(s,t) = x_0(t) + \int_0^s \cos\theta(s',t)\,ds', \tag{2}$$

$$y(s,t) = y_0(t) + \int_0^s \sin\theta(s',t)\,ds'. \tag{3}$$

The trailing-edge position (x_0, y_0) and the tangent angle θ_0 are determined by the force and torque balances for the snake:

$$\int_0^L \rho\partial_{tt}x\,ds = \int_0^L f_x\,ds, \tag{4}$$

$$\int_0^L \rho\partial_{tt}y\,ds = \int_0^L f_y\,ds, \tag{5}$$

$$\int_0^L \rho\mathbf{X}^\perp \cdot \partial_{tt}\mathbf{X}\,ds = \int_0^L \mathbf{X}^\perp \cdot \mathbf{f}\,ds. \tag{6}$$

Here ρ is the mass per unit length and L is the length of the snake. We assume the snake is locally inextensible, and ρ and L are constant in time. $\mathbf{f}$ is the external force per unit length acting on the snake. It includes two parts: the force due to Coulomb friction with the ground [4] and gravity:

$$\begin{aligned}\mathbf{f} = \rho g\cos\alpha[-\mu_t(\widehat{\partial_t\mathbf{X}}\cdot\hat{\mathbf{n}})\hat{\mathbf{n}} - \{\mu_f H(\widehat{\partial_t\mathbf{X}}\cdot\hat{\mathbf{s}})\\ + \mu_b[1 - H(\widehat{\partial_t\mathbf{X}}\cdot\hat{\mathbf{s}})]\}(\widehat{\partial_t\mathbf{X}}\cdot\hat{\mathbf{s}})\hat{\mathbf{s}}] - \rho g G_\alpha.\end{aligned} \tag{7}$$

Here we use the Heaviside function $H(\cdot)$ to allow for different frictional forces in the $\hat{\mathbf{s}}$ and $-\hat{\mathbf{s}}$ directions, and $G_\alpha = (\sin\alpha, 0)^T$ represents the component of gravity in the downhill $(-x)$ direction. The hats denote normalized vectors, and we define $\widehat{\partial_t\mathbf{X}}$ to be zero when the snake velocity is zero. The friction coefficients are μ_f, μ_b, and μ_t for motions in the forward $(\hat{\mathbf{s}})$, backward $(-\hat{\mathbf{s}})$, and transverse $(\pm\hat{\mathbf{n}})$ directions, respectively. Without loss of generality we take $\mu_f \leqslant \mu_b$, so the forward direction has the smaller friction coefficient if it is unequal in the forward and backward directions.

We prescribe the curvature $\kappa(s,t)$ as a time-periodic function with period T and nondimensionalize Eqs. (4)–(6) by length L, time T, and mass ρL. We then obtain

$$\frac{L}{gT^2}\int_0^1 \partial_{tt}x\,ds = \int_0^1 f_x\,ds, \tag{8}$$

$$\frac{L}{gT^2}\int_0^1 \partial_{tt}y\,ds = \int_0^1 f_y\,ds, \tag{9}$$

$$\frac{L}{gT^2}\int_0^1 \mathbf{X}^\perp \cdot \partial_{tt}\mathbf{X}\,ds = \int_0^L \mathbf{X}^\perp \cdot \mathbf{f}\,ds. \tag{10}$$

We neglect the snake's inertia for simplicity, as $L/gT^2 \ll 1$ is the typical range for steady snake locomotion observed in nature [4]. The ratio is small because T, the period of the snake's motion, is typically large relative to $\sqrt{L/g}$. This allows us to simplify the model by setting the left hand sides of (8)–(10) to zero while maintaining a good representation of real snake motions. We then obtain the following dimensionless force and torque equations:

$$\int_0^L f_x ds = 0, \tag{11}$$

$$\int_0^L f_y ds = 0, \tag{12}$$

$$\int_0^L \mathbf{X}^\perp \cdot \mathbf{f} ds = 0, \tag{13}$$

and the dimensionless force $\mathbf{f}$ becomes

$$\mathbf{f} = \cos\alpha[-\mu_t(\widehat{\partial_t \mathbf{X}}\cdot\hat{\mathbf{n}})\hat{\mathbf{n}} - \{\mu_f H(\widehat{\partial_t \mathbf{X}}\cdot\hat{\mathbf{s}}) + \mu_b[1 - H(\widehat{\partial_t \mathbf{X}}\cdot\hat{\mathbf{s}})]\}(\widehat{\partial_t \mathbf{X}}\cdot\hat{\mathbf{s}})\hat{\mathbf{s}}] - G_\alpha. \quad (14)$$

The frictional force tends to zero as α approaches $\pi/2$. On a strictly vertical plane, the frictional force is unable to balance gravity, so planar locomotion is not obtained by the model in this case (however, snakes can ascend vertical crevices in a nonplanar concertina motion [15]).

Given the curvature $\kappa(s,t)$, we solve the three nonlinear equations (11)–(13) at each time t for the three unknowns, $x_0(t), y_0(t)$, and $\theta_0(t)$. Then we obtain the snake's position as a function of time by using Eqs. (1)–(3). We define the cost of locomotion as

$$\eta = \frac{W}{d}, \quad (15)$$

where d is the distance traveled by the snake's center of mass over one period,

$$d=\sqrt{\left(\int_0^1 x(s,1) - x(s,0)\,ds\right)^2 + \left(\int_0^1 y(s,1) - y(s,0)\,ds\right)^2}, \quad (16)$$

and W is the work done by the snake against frictional forces and gravity over one period,

$$W = \int_0^1\int_0^1 -\mathbf{f}(s,t)\cdot\partial_t\mathbf{X}(s,t)\,ds\,dt. \quad (17)$$

Our objective is to find the curvature $\kappa(s,t)$ that minimizes η. We choose the initial orientation of the snake so that its center of mass travels only in the x direction (up the incline) over one period of motion.

We briefly mention the case in which the snake moves down the incline, which is equivalent to setting $\alpha < 0$. In this case the snake can slide down the incline with no change of shape, and the work done by gravity and friction are equal in magnitude and opposite in sign. Thus the cost of locomotion is zero regardless of the frictional parameters. A straight body with $y(s,t) = 0$ experiences purely tangential friction and achieves the fastest speed among possible body shapes.

We focus on the case in which the snake ascends the incline, i.e., $\alpha \geqslant 0$. Here the net tangential friction and gravity both act in the $-x$ direction, and transverse friction acting in the $+x$ direction is necessary to balance the x-force equation. In the following discussion we only consider $\alpha \geqslant 0$ and look for nontrivial $\kappa(s,t)$ to minimize the cost of locomotion.

III. TRIANGULAR WAVE BODY SHAPE

We start with a triangular wave body motion. It was studied on a level plane in [26], and the snake's position, angle, velocity, and work can all be obtained analytically. The motion is useful to consider because it embodies many aspects of more general traveling-wave motions, while the shape dynamics are easy to understand.

The motion is defined by prescribing the position of the snake body as a triangular wave,

$$y(s,t) = A \fint \mathrm{sgn}\{\sin[2\pi(s+t)]\}\,ds. \quad (18)$$

Here $A = |dy/ds| = |\sin\theta(s,t)| \leqslant 1$ [$\theta(s,t)$ is the angle of the tangent to the snake's body], so A is the absolute value of the sine of the angle that the body sections make with the horizontal. We refer to A as the "magnitude" of the triangular wave motion, and it equals four times the amplitude (the largest distance of the triangular wave from the x axis). The horizontal dash through the integral means that we choose the constant of the integration such that the integrated function $y(s,t)$ has zero mean. Therefore, the triangular wave has zero mean vertical deflection relative to the x axis. The triangular wave has the following unit tangent and normal vectors:

$$\hat{\mathbf{s}} = \begin{pmatrix}\sqrt{1-A^2}\\ A\,\mathrm{sgn}\{\sin[2\pi(s+t)]\}\end{pmatrix},\quad \hat{\mathbf{n}} = \begin{pmatrix}-A\,\mathrm{sgn}\{\sin[2\pi(s+t)]\}\\ \sqrt{1-A^2}.\end{pmatrix}. \quad (19)$$

The force and torque balance equations are satisfied when the snake moves forward with a constant speed U. Then the horizontal and vertical speeds are

$$\partial_t x(s,t) = U,\ \partial_t y(s,t) = A\,\mathrm{sgn}\{\sin[2\pi(s+t)]\}. \quad (20)$$

The net y force and torque for such a motion are identically zero. We determine the horizontal speed U by the x-force balance equation:

$$\int \cos\alpha(-\mu_t\widehat{\partial_t\mathbf{X}}\cdot\hat{\mathbf{n}}n_x - \mu_f\widehat{\partial_t\mathbf{X}}\cdot\hat{\mathbf{s}}s_x) - \sin\alpha\,ds = 0. \quad (21)$$

Since $\mu_f \leqslant \mu_b$ and the tangential velocity is uniformly forward or backward over the whole snake body for the triangular wave, the most efficient motion is obtained when the snake moves forward. Thus, μ_b does not appear in the frictional force in (21). Notice that the tangential frictional force and gravity both have a component in the $-x$ direction, and transverse friction provides a balancing force in the $+x$ direction, up the incline. Solving (21) for U, we obtain

$$U = \frac{\left[A^4\left(\frac{\mu_t}{\mu_f}-1\right)^2 + A^2\left(\frac{\mu_t}{\mu_f}-1\right)\right]\sqrt{1-A^2} - A\frac{\tan\alpha}{\mu_f}\sqrt{1+A^2\left(\frac{\mu_t^2}{\mu_f^2}-1\right)-\frac{\tan^2\alpha}{\mu_f^2}}}{\left[1+A^2\left(\frac{\mu_t}{\mu_f}-1\right)\right]^2 - \frac{\tan^2\alpha}{\mu_f^2}}. \quad (22)$$

The speed of the snake is a function of A, μ_t, μ_f, and α.

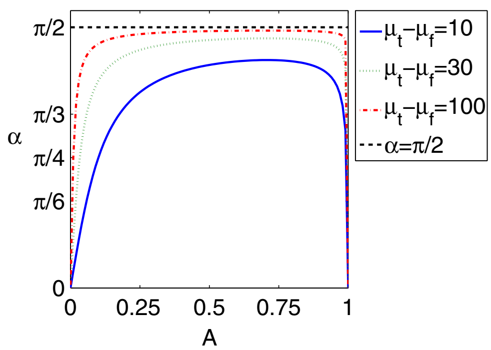

FIG. 2. (Color online) Lines showing the boundaries of the regions of non-negative forward velocity U in the space of A and α for different $\mu_t - \mu_f = 10, 30$, and 100. On the lines, $U = 0$, and below the lines, $U > 0$. The black dashed line shows $\alpha = \pi/2$, giving a vertical incline.

A. Range of α

The speed U is constant along the snake body for the triangular wave motion. As we only consider motions up the incline in this work, U is required to be real and nonnegative, and therefore, the incline angle α must satisfy the following inequality:

$$\alpha \leqslant \arctan[A(\mu_t - \mu_f)\sqrt{1 - A^2}]. \quad (23)$$

Here we use the fact that $A \leqslant 1$ and $\mu_t > \mu_f$. In Fig. 2, we plot the upper bound of α according to inequality (23). For a given value of $\mu_t - \mu_f$, nonnegative speed is obtained for α in the region bounded by a curved line (labeled by $\mu_t - \mu_f$) and the horizontal (A) axis. As μ_t increases, larger transverse friction can be generated for the same A, and therefore, the range of α increases accordingly. As μ_f becomes larger, the tangential motion produces a stronger downhill drag which inhibits the upward motion, so the corresponding α range decreases. When the amplitude A varies from 0 to 1, both the transverse and tangential frictional forces vary, and their x components have opposite sign. As a result, the range of α is nonmonotonic with respect to A. The largest upper bound is obtained at $A = \sqrt{2}/2$.

B. Optima and other results

In the triangular wave motion, the velocity and power are both constant over time, so we can simplify the cost of locomotion as

$$\eta = \frac{W}{d} = \frac{P}{U} = \frac{\int_0^1 -\mathbf{f} \cdot \partial_t \mathbf{X} ds}{U} \quad (24)$$

and obtain

$$\eta = \frac{\cos\alpha}{\sqrt{U^2 + A^2}}\left[A^2(\mu_t - \mu_f)\left(U - 2\sqrt{1 - A^2} - \frac{A^2}{U}\right) + \mu_f U + \frac{\mu_t A^2}{U}\right] + \sin\alpha. \quad (25)$$

We plug the value of U (22) into (25) and minimize η with respect to A. Then in the large-μ_t limit we obtain the optimal cost of locomotion and corresponding amplitude

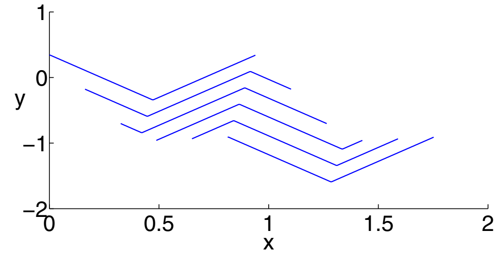

FIG. 3. (Color online) The optimal snake trajectory of the triangular wave body shape over one period obtained with $\alpha = \pi/4$, $\mu_f = 1$, and $\mu_t = 10$.

as

$$\min \eta \longrightarrow (\mu_f \cos\alpha + \sin\alpha)\left[1 + \left(\frac{2\mu_f}{\mu_t}\right)^{1/2}\right], \quad (26)$$

$$A \longrightarrow 2^{1/4}\mu_t^{-1/4}\left(\mu_f^{1/2} + \frac{\tan\alpha}{\mu_f^{1/2}}\right)^{1/2}. \quad (27)$$

We plot the optimal motion with $\alpha = \pi/4$, $\mu_f = 1$, and $\mu_t = 10$ over one period in Fig. 3. We manually offset the body by a constant increment in the $-y$ direction with every snapshot to clearly show the individual bodies, but we note that for the triangular wave motion, the snake's center of mass moves purely along the x axis. The peak of the snake shifts to the left in the figure, which indicates the snake moves slower than the traveling triangular wave. The snake slips transversely in the $-x$ direction to obtain a thrust force in the $+x$ direction that balances the drag forces due to tangential friction and gravity.

In Fig. 4 we plot the optimal A and η with respect to α, μ_t, and μ_f. Our results begin with μ_t below the large-μ_t limit, and as this limit is reached, the results agree with (26) and (27). For each parameter set, we minimize η over A using Eqs. (22) and (25).

We plot A versus μ_t in Fig. 4(a) with fixed $\mu_f = 1$ and vary the parameter α. The asymptotic scaling of $\mu_t^{-1/4}$ is shown with the solid line. The corresponding η and the scaling $(\mu_f/\mu_t)^{1/2}$ (solid line) are plotted in Fig. 4(b). The optimal magnitude A and cost of locomotion η both decrease with larger μ_t. We vary μ_f and α in Figs. 4(c) and 4(d) with fixed $\mu_t = 10\,000$ and plot the optimal A versus μ_f and η versus μ_f, respectively. The analytical solutions of (26) and (27) for $\alpha = 2\pi/5$ are shown with solid lines in both figures, and they agree well with the corresponding numerical results (downward-pointing triangles). The optimal magnitude A achieves its minimum at $\mu_f = \tan\alpha$, while the cost of locomotion η monotonically increases with μ_f as $\partial_{\mu_f}\eta > 0$. When α goes up, the optimal A increases accordingly, and its minimum over μ_f shifts to larger μ_f [Fig. 4(c)]. But the cost of locomotion varies nonmonotonically with α. We can rewrite (27) as

$$\min \eta \longrightarrow \sqrt{\mu_f^2 + 1}\,\sin\left(\alpha + \arcsin\frac{\mu_f}{\sqrt{\mu_f^2 + 1}}\right) \times \left[1 + \left(\frac{2\mu_f}{\mu_t}\right)^{1/2}\right]. \quad (28)$$

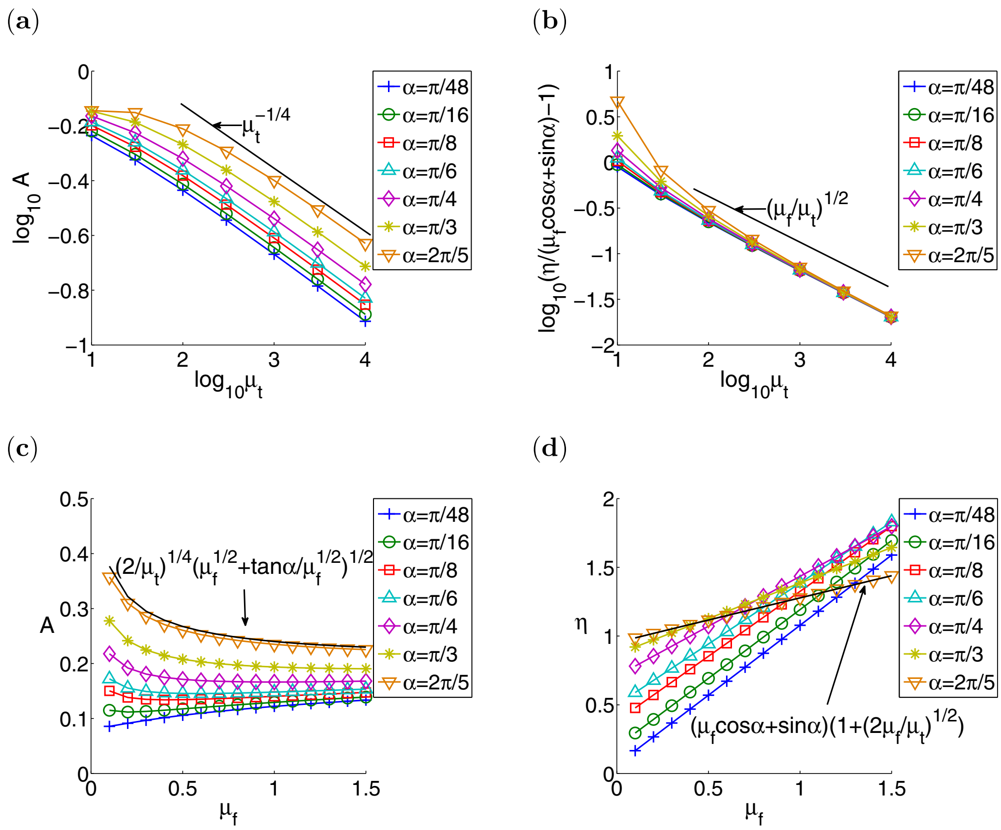

FIG. 4. (Color online) Scaling laws of the triangle wave optima. (a) $\log_{10} A$ vs $\log_{10} \mu_t$ with various α and fixed $\mu_f = 1$. The solid line indicates the scaling $\mu_t^{-1/4}$. (b) $\log_{10}[\eta/(\mu_f \cos\alpha + \sin\alpha) - 1]$ vs $\log_{10} \mu_t$ with various α and fixed $\mu_f = 1$. The solid line shows the scaling $(\mu_f/\mu_t)^{1/2}$. (c) A vs μ_f with various α and fixed $\mu_t = 10\,000$. The solid line is the asymptotic solution $A = 2^{1/4}\mu_t^{-1/4}(\mu_f^{1/2} + \tan\alpha/\mu_f^{1/2})^{1/2}$, obtained with $\alpha = 2\pi/5$. (d) η vs μ_f with various α and fixed $\mu_t = 10\,000$. The solid line shows the asymptotic optima $\eta = (\mu_f \cos\alpha + \sin\alpha)[1 + (2\mu_f/\mu_t)^{1/2}]$ with $\alpha = 2\pi/5$.

The least efficient optimum is obtained when

$$\alpha^* = \frac{\pi}{2} - \arcsin \frac{\mu_f}{\sqrt{\mu_f^2 + 1}}. \tag{29}$$

We call α^* the critical incline angle. The optimal snake moves more efficiently when the incline is either shallower or steeper than the incline at the critical angle. The critical incline angle α^* only depends on the tangential friction coefficient and becomes smaller as μ_f increases. On a steeper slope, more work is done against gravity and less work is done against forward friction for a given distance traveled. Thus, when μ_f increases, efficiency can be improved by making the slope steeper (and adjusting the amplitude to achieve the optimum at the new set of parameters).

To better understand the effects of the parameters μ_t, μ_f, and α, we plot the costs of locomotion due to transverse friction and tangential friction versus A in Fig. 5. We decompose the cost of locomotion (25) into three parts:

$$\eta = \eta_t + \eta_f + \eta_g, \tag{30}$$

where

$$\eta_t = \frac{\cos\alpha}{\sqrt{U^2 + A^2}}\left(UA^2\mu_t - 2A^2\sqrt{1 - A^2}\mu_t - \frac{A^4\mu_t}{U} + \frac{A^2\mu_t}{U}\right), \tag{31}$$

$$\eta_f = \frac{\cos\alpha}{\sqrt{U^2 + A^2}}\left[U\mu_f(1 - A^2) + 2A^2\sqrt{1 - A^2}\mu_f + \frac{A^4\mu_f}{U}\right], \tag{32}$$

$$\eta_g = \sin\alpha \tag{33}$$

are the costs due to transverse friction, forward tangential friction, and gravity, respectively.

In Fig. 5, we vary one of the parameters μ_t, μ_f, and α in turn and keep the other two fixed. We use solid lines for the transverse friction and dashed lines for the tangential friction in all panels. In general, as the magnitude A becomes larger, the cost due to transverse friction decreases while the cost due to tangential friction increases. The optimal η is obtained when the slopes of the two costs are equal in magnitude and opposite in sign. η_g is independent of A so it does not play a role in determining the optimal A.

In Fig. 5(a), the sums of the costs of the frictional forces become smaller as μ_t increases. Thus, the optimal η decreases as well, as shown in Fig. 4(b). For a given motion (a given A), the slope of the tangential cost is almost unchanged as μ_t goes up, while the magnitude of the slope of the transverse cost quickly decays. The point where the two slopes balance shifts to the left at larger μ_t. The optimal motion is thus obtained at a

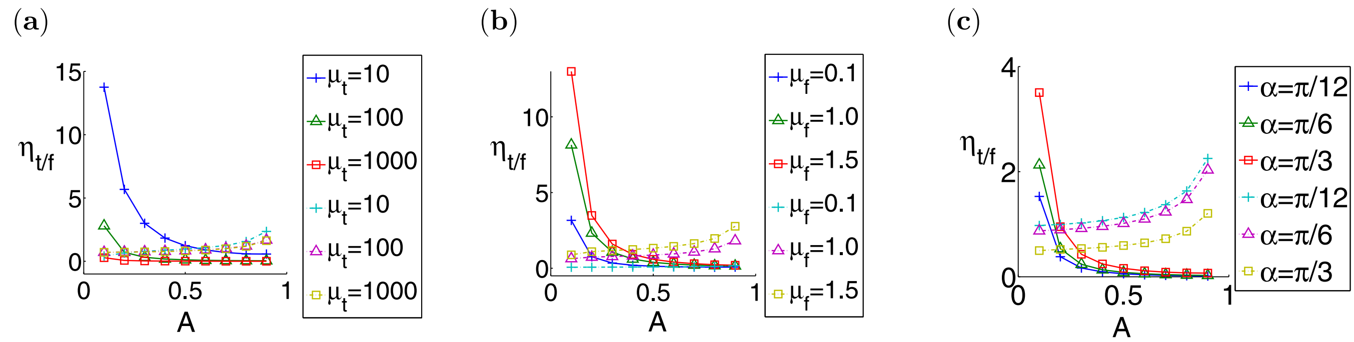

FIG. 5. (Color online) Costs of locomotion ($\eta_{t/f}$) due to transverse friction (solid lines) and tangential friction (dashed lines) vs A with (a) various μ_t and fixed $\alpha = \pi/4$ and $\mu_f = 1$, (b) various μ_f and fixed $\alpha = \pi/4$ and $\mu_t = 30$, and (c) various α and fixed $\mu_t = 100$ and $\mu_f = 1$.

smaller amplitude as μ_t increases. We show the results only for $\alpha = \pi/4$ and $\mu_f = 1$ in the figure, but the same phenomenon holds for all α and μ_f. Physically, as the transverse coefficient increases, the snake can obtain the same amount of forward force from transverse friction with less deflection of the body and less slipping in the transverse direction, and the cost of the tangential friction is reduced as well due to a shorter path traveled. Thus, the total cost of locomotion η decreases with μ_t.

We show in Fig. 5(b) that the costs due to transverse friction and tangential friction both increase as μ_f increases. When the friction coefficient μ_f is larger, the snake of the same deflection experiences a stronger downward drag caused by tangential friction, increasing the slipping and, consequently, the work done against transverse friction as well. The optimal magnitude A varies nonmonotonically with μ_f, as shown in Fig. 4(c). The slopes of both costs increase with μ_f for given A. When $\mu_f < \tan\alpha$, the point where the two slopes are equal in magnitude shifts to smaller A as μ_f increases. When $\mu_f > \tan\alpha$, the balanced point shifts to larger A.

In Fig. 5(c), we fix $\mu_t = 100$ and $\mu_f = 1$ and vary the incline angle α. The cost due to gravity is $\sin\alpha$ for the triangular wave motion and thus always increases with α. Meanwhile, the tangential cost decreases with α while the transverse cost increases. The competition of these three costs makes η nonmonotonic with α, as shown in Fig. 4(d). For a given motion, the slope of the tangential cost with respect to A is nearly unchanged as the incline becomes steeper. However, the magnitude of the slope of the transverse cost increases with α, so a point with a given slope of the transverse cost shifts to larger A as α increases. Therefore, the point where two slopes are equal and opposite shifts to larger A as α increases, so the optimal A in Figs. 4(a) and 4(c) grows with α.

IV. SINUSOIDAL BODY SHAPE

We now consider an alternative, sinusoidal snake motion to check the dependence of our results on the snake shape. We again determine the snake shape which minimizes η for a given parameter set $(\mu_t, \mu_f, \mu_b, \alpha)$.

We define the body shape by prescribing its curvature as a sinusoidal function with t period 1:

$$\kappa(s,t) = K\cos(n\pi s + 2\pi t). \tag{34}$$

This body shape, with sinusoidal curvature, has been called a "serpenoid curve" by Hirose [2,29] and others in robotics. We fix the wave number n in this work and look for the optimal constant K to minimize η for a given $(\mu_t, \mu_f, \mu_b, \alpha)$. Later, we show that although the wave number n affects the optimal value of K, it does not change the dependence of the optimal K on the other parameters. We fix $n = 6$ in this section since, for a horizontal plane, the lowest cost of locomotion is obtained in the limit of large wave numbers according to [26], and $n = 6$ approximates this limit while only requiring a moderate number of grid points in arc length along the snake to discretize the equations accurately.

A. Numerical method

We find the optimal η on a sequence of one-dimensional meshes of K values with decreasing spacing. Each mesh in the sequence is centered near the minimizer from the previous coarser mesh. The fourth mesh used has a mesh size of 10^{-3}. We then use a quadratic curve to fit the data around the minimum point on the fourth mesh and obtain the optimal K based on a final fifth mesh, with mesh width 10^{-6}. In [26] Alben used a Broyden-Fletcher-Goldfarb-Shanno (BFGS) algorithm [30] to minimize the cost of locomotion when the curvature is described by a double-series expansion with 45 parameters. In this work we optimize over only a single parameter (the amplitude) for a given shape. We find that a direct search over the parameter space is typically fast enough since η varies smoothly with K in the regime of physically admissible, nonoverlapping shapes.

The algorithm requires fast routines to evaluate η. Here we describe our numerical scheme that solves for the work, distance, and cost of locomotion. Given the curvature $\kappa(s,t)$, we solve the three nonlinear equations (11)–(13) at each time step, over a period, for the three unknowns, $x_0(t), y_0(t)$, and $\theta_0(t)$. Then we use Eqs. (1)–(3) to compute $x(t), y(t)$, and $\theta(t)$ and obtain d, W, and η over one period.

We discretize the period interval uniformly with m time points: $\{0, 1/m, \ldots, 1 - 1/m\}$. We rewrite Eqs. (11)–(13) as equations in unknowns $\{\partial_t x_0, \partial_t y_0, \partial_t \theta_0\}$ by taking time derivatives on both sides. Therefore, at each time level, we solve for $\{\partial_t x_0, \partial_t y_0, \partial_t \theta_0\}$ and then integrate to obtain $\{x_0, y_0, \theta_0\}$. The advantage of replacing x_0, y_0, and θ_0 with their time derivatives as variables is that it avoids the numerical

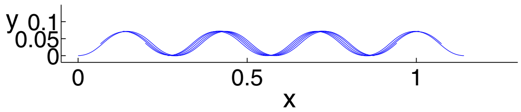

FIG. 6. (Color online) The optimal snake trajectory of the sinusoidal wave body shape over one period obtained with $\alpha = \pi/4$, $\mu_f = 1$, and $\mu_t = 10$.

error in computing the discrete time derivatives and decreases the computational cost by decoupling a large system of $3m$ equations in $3m$ unknowns into m decoupled systems each containing only 3 equations in 3 unknowns [26].

We design a time-marching scheme which is second order accurate in both time and space to solve for $\{\partial_t x_0, \partial_t y_0, \partial_t \theta_0\}$. At each time level i, we use Newton's method with a finite-difference Jacobian matrix as described in [26] to solve the nonlinear equations for $\{\partial_t x_0^i, \partial_t y_0^i, \partial_t \theta_0^i\}$. To evaluate the function values in Newton's method, the current step position and angle $\{x_0^i, y_0^i, \theta_0^i\}$ are required, and guesses are obtained by the forward Euler method. After we obtain the current time derivatives $\{\partial_t x_0^i, \partial_t y_0^i, \partial_t \theta_0^i\}$, we update the position and angle by integrating $\{\partial_t x_0, \partial_t y_0, \partial_t \theta_0\}$ from $t = 0$ to $t = i/m$. We can iterate the same procedure until a certain accuracy is obtained. We find that second-order temporal accuracy is achieved by iterating only once. The initial condition $\{\partial_t x_0^0, \partial_t y_0^0, \partial_t \theta_0^0\}$ is obtained by setting $\{x_0^0, y_0^0, \theta_0^0\}$ to $\{0,0,0\}$ and using Newton's method.

B. Optima and other results

We first consider the case $\mu_t \gg \mu_f$. Here the tangential motion is purely in the forward direction for the sinusoidal wave motion. Therefore, as for the triangular wave, the μ_b term drops out of the force law, and the parameter space is reduced to $\{\mu_t, \mu_f, \alpha\}$. We plot the optimal snake trajectory with parameters $\alpha = \pi/4$, $\mu_f = 1$, and $\mu_t = 10$ over one period in Fig. 6. The snake moves from left to right, and its center of mass moves mainly along the x direction.

In Fig. 7, we vary μ_t, μ_f, and α and plot the optimal K and cost of locomotion η versus these parameters. Some data points are ignored because there is no solution with non-negative x velocity for the corresponding parameter values. We fix $\mu_f = 1$ and plot the optimal K and η versus μ_t with various α in Figs. 7(a) and 7(b). In Figs. 7(c) and 7(d), we fix $\mu_t = 10\,000$ and vary μ_f from 0.1 to 2 with different α. We find that the optima for the sinusoidal wave motion satisfy essentially the same scaling laws as the triangular wave motion in (26) and (27). The cost of locomotion is the same as (26), and the amplitude K is scaled by an extra factor $\sqrt{2}n\pi$, yielding a deflection amplitude that agrees with (27).

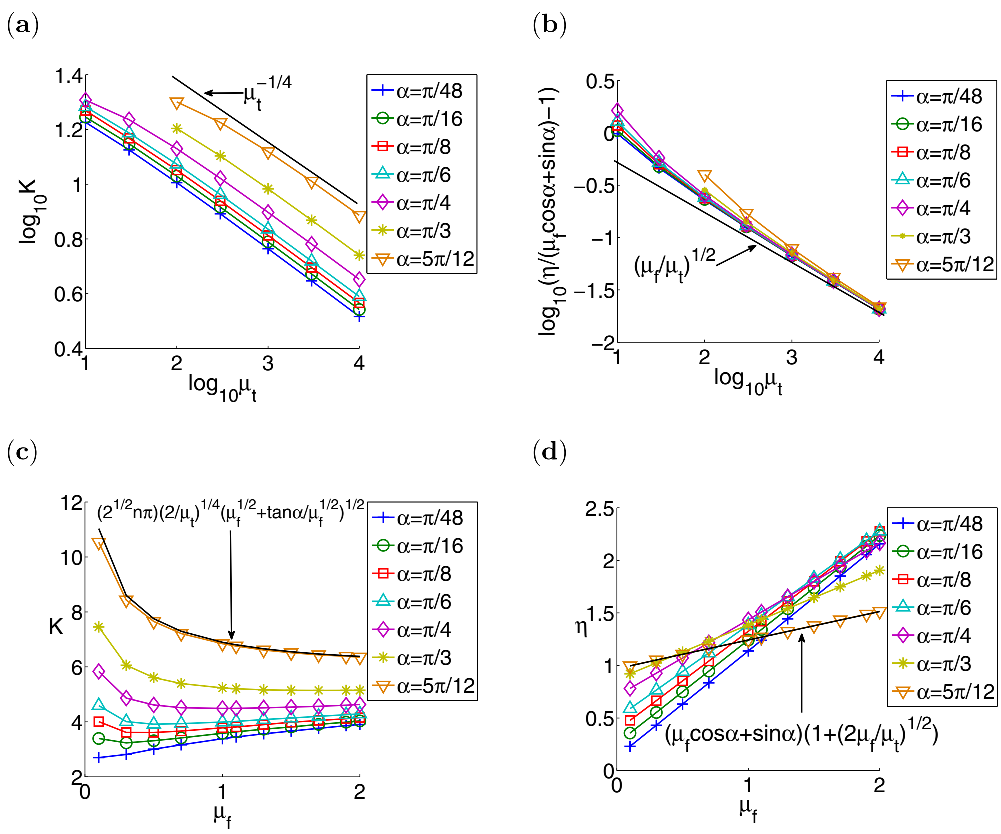

FIG. 7. (Color online) Scaling laws for the sinusoidal wave optima. (a) $\log_{10} K$ vs $\log_{10} \mu_t$ with various α and fixed $\mu_f = 1$. The solid line shows the scaling law $\mu_t^{-1/4}$. (b) $\log_{10}[\eta/(\mu_f \cos\alpha + \sin\alpha) - 1]$ vs $\log_{10} \mu_t$ with various α and fixed $\mu_f = 1$. The solid line denotes the scaling $(\mu_f/\mu_t)^{1/2}$. (c) K vs μ_f with various α and fixed $\mu_t = 10\,000$. The solid line is the analytical optimum $K = \sqrt{2}n\pi(2/\mu_t)^{1/4}(\mu_f^{1/2} + \tan\alpha/\mu_f^{1/2})^{1/2}$ obtained with $\alpha = 5\pi/12$. (d) η vs μ_f with various α and fixed $\mu_t = 10\,000$. The solid line is the graph of the optimal $\eta = (\mu_f \cos\alpha + \sin\alpha)[1 + (2\mu_f/\mu_t)^{1/2}]$ with $\alpha = 5\pi/12$.

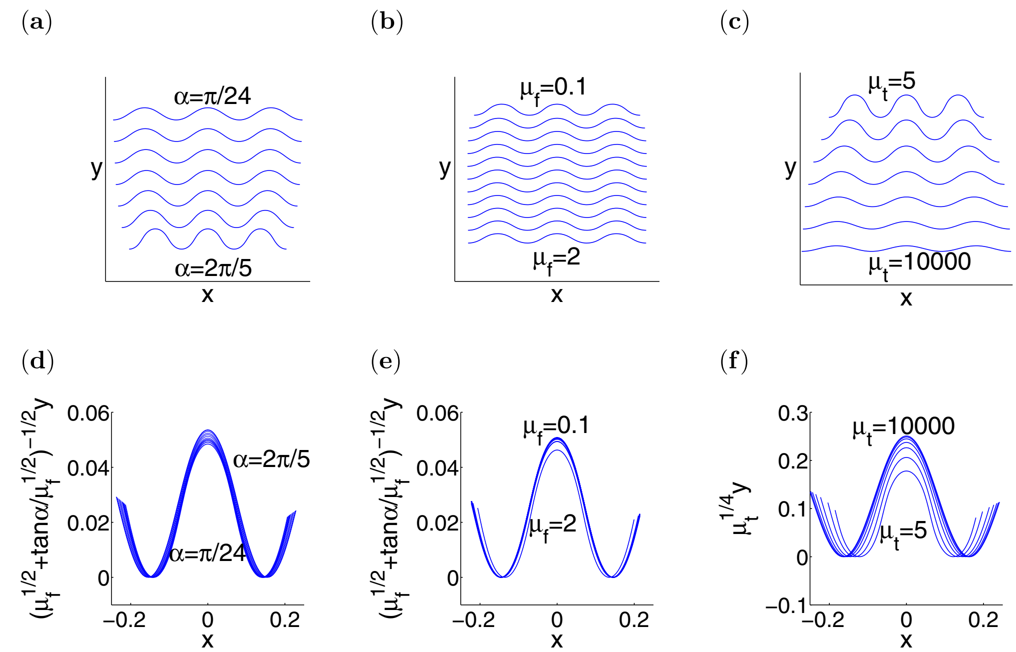

FIG. 8. (Color online) Optimal snake shapes at the instant $t = 0$ for (a) $\alpha = \pi/24$, $\pi/12$, $\pi/8$, $\pi/6$, $\pi/4$, $\pi/3$, $2\pi/5$, $\mu_f = 1$, and $\mu_t = 100$; (b) μ_f =0.1, 0.3, 0.5, 0.7, 0.9, 1.0, 1.2, 1.4, 1.6, 1.8, 2.0, $\alpha = \pi/4$, and $\mu_t = 100$; and (c) μ_t =5, 10, 100, 500, 1000, 5000, 10 000, $\alpha = \pi/4$, and $\mu_f = 1$. (d) The deflection of the body rescaled by $(\mu_f^{1/2} + \tan\alpha/\mu_f^{1/2})^{-1/2}$ corresponding to (a). (e) The deflection rescaled by $(\mu_f^{1/2} + \tan\alpha/\mu_f^{1/2})^{-1/2}$ for (b). (f) The deflection rescaled by $\mu_t^{1/4}$ with the same parameters as (c).

We show the optimal snake body shapes corresponding to different α, μ_f, and μ_t in Figs. 8(a), 8(b), and 8(c), respectively. We displace the different bodies vertically so that they are easier to distinguish. In Figs. 8(d), 8(e), and 8(f), we rescale the deflections of the optimal shapes with α, μ_f, and μ_t according to the scaling law for the optimal amplitude (27). The centers of mass for all bodies are located at the origin. Here we zoom in on the portion of the body nearest the center. We find a good collapse of the bodies after rescaling.

In the regime where μ_t and μ_f are comparable, the sinusoidal body shape model may not yield forward motion. For snake locomotion on a level plane, Alben [26] found that when $\mu_t/\mu_f \lesssim 6$, the optimal snake shape is no longer a retrograde traveling wave. He identified a set of locally optimal motions and classified some of them as ratchetting motions. When the snake climbs uphill and μ_t is small, the traveling wave may not be able to provide enough uphill thrust to balance gravity and the drag due to forward motion. The snake may therefore use locomotion modes other than slithering to maintain its position on the incline. For example, concertina locomotion is often observed for snakes moving inside an inclined tunnel. Marvi and Hu [15] found that some snakes can resist sliding by varying their frictional interactions with the ground. They will lift part of the body, reduce the contact with the ground to several localized regions, and orient their scales to increase the frictional coefficients for a portion of the body. In this situation, μ_t and μ_f are not uniform along the whole body. A planar model does not yield net snake locomotion on steep inclines when the ratio of the transverse-to-tangential friction coefficient is small. Our future work may consider three-dimensional motions to better understand this interesting parameter regime.

V. ASYMPTOTIC ANALYSIS

A. Optimal shape dynamics

We now analytically determine how the optimal snake motion depends on the parameters $\{\mu_t,\mu_f,\alpha\}$, thus providing theoretical confirmation of our previous results and extending them to general shapes in the large-μ_t regime. We assume that the mean direction of the motion is aligned with the x axis and the deflections along the y direction are small, i.e., $|y|$ and all of its temporal and spatial derivatives $|\partial_t y|, |\partial_s y|, |\partial_t^2 y|, \ldots,$ are $O(\mu_t^\beta)$ for some negative β. We also assume that the tangential motion is only in the forward direction to simplify the derivation. We first expand each term in the force and torque balance equations in powers of $|y|$ and retain only the terms which are dominant at large μ_t. A detailed discussion of the expansion of each term can be found in [26]. If we only keep the lowest powers in y from each expression, the x-force balance equation becomes

$$\int_0^1 -\cos\alpha\left[\mu_f + \mu_t\partial_s y\left(\partial_s y - \frac{\partial_t y}{U}\right)\right] - \sin\alpha\, ds = 0, \tag{35}$$

where $U(t) \equiv \overline{\partial_t x(s,t)}$ is the s-averaged horizontal velocity. The three terms in the integral represent the drag due to forward friction, the thrust due to transverse friction, and gravity, respectively. We note that both the tangential friction and gravity forces act in the $-x$ direction, and transverse friction is essential to maintain the x-force balance. In [26] it is shown that for large μ_t, a minimizer of the cost of locomotion should approximate a traveling-wave motion. Therefore, we pose the shape dynamics as

$$y(s,t) = g(s + U_w t), \tag{36}$$

which is a traveling wave with a prescribed wave speed U_w. U_w is different from $U(t)$ in general, for otherwise, the snake moves purely tangentially with no transverse motion. Here g is a periodic function with period U_w (so y has t period 1). We obtain an equation for U in terms of U_w and g by substituting (36) into (35):

$$-\mu_f \cos\alpha - \mu_t \cos\alpha \left(1 - \frac{U_w}{U}\right)\langle g'(s + U_w t)^2\rangle = \sin\alpha, \tag{37}$$

where $\langle g'(s + U_w t)^2\rangle \equiv \int_0^1 g'(s + U_w t)^2\, ds$. As $\alpha \to \pi/2$, $\cos\alpha \to 0$, and no frictional force occurs. Therefore, in the limit $\alpha \to \pi/2$, we require $\mu_t \to \infty$ such that $\mu_t \cos\alpha \to \infty$; that is, the speed at which α tends to $\pi/2$ depends on the speed at which μ_t tends to infinity. This requirement is similar to the upper bound of α in the triangular wave motion to obtain forward motion. As $\mu_t \cos\alpha \to \infty$, Eq. (37) holds with $(1 - U_w/U) \to 0^-$. The traveling wave moves backward along the snake at speed U_w while the snake moves forward at a speed U slightly less than U_w. Therefore, the snake slips transversely to itself, which provides an uphill thrust to balance gravity and the drag due to tangential friction.

In [26] it is shown that one must expand the terms in the force balance equation in higher powers of $|y|$ to obtain an optimal motion. We do so, again assuming $y = g(s + U_w t)$. Then the force balance equation becomes

$$\cos\alpha \left\{\mu_f + \mu_t \left[\left(1 - \frac{U_w}{U}\right)\langle g'(s + U_w t)^2\rangle + \frac{1}{2}\langle g'(s + U_w t)^2\rangle^2\right]\right\} = -\sin\alpha, \tag{38}$$

and the cost of locomotion is

$$\eta \sim \sin\alpha + \int_0^1 \cos\alpha\,\mu_f \left(1 + \frac{1}{2}\langle g'^2\rangle\right) + \cos\alpha\,\mu_t \left(1 - \frac{U_w}{U} + \frac{1}{2}\langle g'^2\rangle\right)^2 \langle g'^2\rangle + O(\mu_f |g|^4, \mu_t |g|^8)\, dt. \tag{39}$$

Equation (39) is shown in a simplified form, using the result that $(1 - U_w/U) \to 0$ as $\mu_t \cos\alpha \to \infty$. We substitute Eq. (38) into (39) and obtain

$$\eta = 1 \Big/ \int_0^1 \frac{1}{\sin\alpha + \cos\alpha\,\mu_f\left(1 + \frac{1}{2}\langle g'^2\rangle\right) + \frac{\cos\alpha(\mu_f + \tan\alpha)^2}{\mu_t \langle g'^2\rangle} + O(\mu_f |g|^4, \mu_t |g|^8)} dt. \tag{40}$$

If we approximate $\langle g'(s + U_w t)^2\rangle$ as constant in time, we obtain

$$\eta = \mu_f \cos\alpha + \sin\alpha + \frac{\mu_f \cos\alpha}{2}\langle g'^2\rangle + \frac{\cos\alpha(\mu_f + \tan\alpha)^2}{\mu_t \langle g'^2\rangle} + O(\mu_f |g|^4, \mu_t |g|^8), \tag{41}$$

which is minimized for

$$\langle g'^2\rangle^{1/2} = 2^{1/4}\mu_t^{-1/4}\left(\mu_f^{1/2} + \frac{\tan\alpha}{\mu_f^{1/2}}\right)^{1/2}, \tag{42}$$

and the corresponding optimal cost of locomotion is

$$\eta = (\mu_f \cos\alpha + \sin\alpha)\left[1 + \left(\frac{2\mu_f}{\mu_t}\right)^{1/2}\right]. \tag{43}$$

In the triangular wave motion, we have

$$y(s,t) = g(s + t) = A \int \operatorname{sgn}\{\sin[2\pi(s + t)]\} ds. \tag{44}$$

By using (42), we obtain

$$A = \langle g'^2\rangle^{1/2} = 2^{1/4}\mu_t^{-1/4}\left(\mu_f^{1/2} + \frac{\tan\alpha}{\mu_f^{1/2}}\right)^{1/2}, \tag{45}$$

which is consistent with the analytical result we obtained in (27).

B. Optimal curvature analysis

For a more general body shape, to satisfy the y-force balance and torque balance, we instead prescribe the curvature $\kappa(s,t)$ and obtain $x(s,t)$, $y(s,t)$, and $\theta(s,t)$ from Eqs. (1)–(3). We now correct the above analysis to satisfy all three equations. We again assume that the deflection from the x axis is small, and we decompose $y(s,t)$ as

$$y(s,t) = y_0(t) + \int_0^s \sin\theta(s',t)ds' \tag{46}$$

$$= y_0(t) + \int_0^s \theta(s',t)ds' + O(y^3) \tag{47}$$

$$= y_0(t) + \int_0^s \theta_0(t) + \int_0^{s'} \kappa(s'',t)ds''ds' + O(y^3) \tag{48}$$

$$= y_0(t) + s\theta_0(t) + \int_0^s \int_0^{s'} \kappa(s'',t)ds''ds' + O(y^3) \tag{49}$$

$$\equiv Y(t) + sR(t) + k(s,t) + O(y^3). \tag{50}$$

Prescribing the curvature is the equivalent of prescribing $k(s,t)$. We set

$$k(s,t) = g(s + U_w t) \tag{51}$$

so y is similar to the form given before, with two additional terms: vertical translation $Y(t)$ and rotation $R(t)$. We determine Y and R by expanding the y force equation (12) and torque balance equation (13) to leading order in $|y|$ and obtain

$$\int_0^1 \left(-\frac{U_w}{U} + 1 + \frac{1}{2}\langle g'^2\rangle\right) g' - \frac{Y'}{U} - \frac{R's}{U} + R\, ds = 0, \tag{52}$$

$$\int_0^1 s\left[\left(-\frac{U_w}{U} + 1 + \frac{1}{2}\langle g'^2\rangle\right) g' - \frac{Y'}{U} - \frac{R's}{U} + R\right] ds = 0. \tag{53}$$

We solve (52) and (53) for Y and R:

$$\frac{Y'}{U} - R = 4\Gamma - 6\Lambda, \tag{54}$$

$$\frac{R'}{U} = 12\Lambda - 6\Gamma. \tag{55}$$

$$\Lambda \equiv \left(-\frac{U_w}{U} + 1 + \frac{1}{2}\langle g'^2\rangle\right)\langle s g'\rangle, \tag{56}$$

$$\Gamma \equiv \left(-\frac{U_w}{U} + 1 + \frac{1}{2}\langle g'^2\rangle\right)\langle g'\rangle. \tag{57}$$

We then express the x-force balance equation in terms of Y and R and obtain

$$\int_0^1 -\cos\alpha\left[\mu_f + \mu_t\left(-\frac{U_w}{U} + 1 + \frac{1}{2}\langle g'^2\rangle\right) g'^2 + \mu_t\left(-\frac{Y'}{U} - \frac{R's}{U} + R\right) g'\right] - \sin\alpha\, ds = 0. \tag{58}$$

Substituting (54) and (55) into (58), we solve for U in terms of g:

$$\frac{U_w}{U} = 1 + \frac{1}{2}\langle g'^2\rangle + \frac{\mu_f + \tan\alpha}{\mu_t[\langle g'^2\rangle - \langle g'\rangle^2 - 3(\langle g'\rangle - 2\langle s g'\rangle)^2]}. \tag{59}$$

The cost of locomotion η then becomes

$$\eta = 1\Big/\int_0^1 \frac{1}{\sin\alpha + \cos\alpha\left[\mu_f\left(1 + \frac{1}{2}\langle g'^2\rangle\right) + \frac{(\mu_f + \tan\alpha)^2}{\mu_t[\langle g'^2\rangle - \langle g'\rangle^2 - 3(\langle g'\rangle - 2\langle s g'\rangle)^2]}\right]} dt. \tag{60}$$

Following [26], we expand g' in a basis of Legendre polynomials L_k for any fixed time t. The Legendre polynomials are orthonormal functions with unit weight on [0,1]. They satisfy the relations

$$\int_0^1 L_i L_j ds = \delta_{ij};\ L_0 = 1,\ L_1 = \sqrt{12}(s - 1/2), \ldots. \tag{61}$$

We write g' as

$$g'(s + U_w t) = \sum_{k=0}^{\infty} c_k(t) L_k(s), \tag{62}$$

and we have

$$\langle g'^2\rangle = \sum_{k=0}^{\infty} c_k(t)^2, \tag{63}$$

$$\langle g'\rangle^2 = c_0(t)^2, \tag{64}$$

$$3(\langle g'\rangle - 2\langle s g'\rangle)^2 = c_1(t)^2. \tag{65}$$

Inserting into (60), we obtain

$$\eta = 1\Big/\int_0^1 \frac{1}{\cos\alpha\left[1+\frac{1}{2}\left(c_0(t)^2+c_1(t)^2+\sum_{k=2}^{\infty}c_k(t)^2\right)+\frac{(\mu_f+\tan\alpha)^2}{\mu_t\sum_{k=2}^{\infty}c_k(t)^2}\right]+\sin\alpha}dt. \quad (66)$$

Therefore, η is minimized for

$$c_0(t)=0;\ c_1(t)=0;\ \sum_{k=2}^{\infty}c_k(t)^2=\sqrt{2}\mu_t^{-1/2}\left(\mu_f^{1/2}+\frac{\tan\alpha}{\mu_f^{1/2}}\right). \quad (67)$$

If a periodic function $g(s+U_w t)$ satisfies (67) for all t, this is the curvature function which minimizes the cost of locomotion. The corresponding cost of locomotion is

$$\eta \longrightarrow (\mu_f\cos\alpha+\sin\alpha)\left[1+\left(\frac{2\mu_f}{\mu_t}\right)^{1/2}\right]. \quad (68)$$

Finally, we define the amplitude of the snake motion as

$$A \equiv \left(\frac{1}{U_w}\int_0^{U_w} g'(x)^2 dx\right)^{1/2}. \quad (69)$$

Then we obtain

$$\langle g'^2\rangle = A^2 + O(U_w), \quad (70)$$

$$\langle g'\rangle = O(U_w), \quad (71)$$

$$\langle s g'\rangle = O(U_w). \quad (72)$$

Therefore, in the limit of $U_w \to 0$, (67) holds with the optimal

$$A = 2^{1/4}\mu_t^{-1/4}\left(\mu_f^{1/2}+\frac{\tan\alpha}{\mu_f^{1/2}}\right)^{1/2}. \quad (73)$$

The derivation of (70)–(72) can be found in an appendix of [26]. We notice that when $\alpha = 0$ and $\mu_f = 1$, $\eta \to 1+\sqrt{2}\mu_t^{-1/2}$ and the optimal $A \to 2^{1/4}\mu_t^{-1/4}$, which are consistent with the optimal solutions of snake motion on a level plane, derived in [26].

For the sinusoidal wave motion, we prescribed the curvature of the sinusoidal wave as

$$\kappa(s,t) = K\cos(n\pi s + 2\pi t), \quad (74)$$

and according to (69), we obtain the amplitude A,

$$A = \frac{K}{\sqrt{2}n\pi}. \quad (75)$$

Therefore, the magnitude of the sinusoidal wave K scales as

$$K = (\sqrt{2}n\pi)(2^{1/4}\mu_t^{-1/4})\left(\mu_f^{1/2}+\frac{\tan\alpha}{\mu_f^{1/2}}\right)^{1/2}, \quad (76)$$

which is consistent with our numerical results.

We now discuss the case in which the snake's net displacement is not solely in the x direction, up the incline, but instead has a nonzero component in the y direction, across the incline. The above analysis and [26] show that in the limit of large μ_t, the minimum cost of locomotion is achieved when the curvature is any traveling-wave function, in the limit of vanishing wavelength and with amplitude tending to zero like $\mu_t^{-1/4}$. For all such optimal motions, the snake moves along a straight-line path. Let the distance traveled by the center of mass over one period be d, with x and y displacements d_x and d_y, so $d = \sqrt{d_x^2+d_y^2}$. We may redefine η as W/d_x now, so only the distance traveled up the incline is considered useful. We also set $\eta = +\infty$ if $d_x < 0$ to avoid the trivial case in which the snake travels down the incline, which we discussed in Sec. II. Our previous results continue to hold with this definition of η because we set the initial orientation of the snake so that its center of mass travels only in the x direction and $d = d_x \geqslant 0$ in all cases. Now if $d_y \geqslant 0$, we first claim that the optimal motions in the large-μ_t limit still follow straight-line paths. Any nonstraight path with the same beginning and end points would have a greater arc length and thus require more work done against forward friction for the same distance traveled by the snake's center of mass. For a straight-line path, the work against transverse friction vanishes [corresponding to η in Eq. (43) in the limit of large μ_t], so it can not be decreased for the nonstraight path. Work against gravity is the same for the straight and nonstraight paths since d_x is the same. Therefore, the straight-line path is the optimal path to minimize η. Now we show that the η-minimizing path is a straight-line path with $d_y = 0$. η is now a generalized version of Eq. (43):

$$\eta \to \mu_f\cos\alpha\frac{d}{d_x}+\sin\alpha \quad \text{as} \quad \mu_t\to\infty, \quad (77)$$

and it is minimized when $d_y = 0$ and $d = d_x$. In short, nonzero d_y increases the work against forward tangential friction without any compensating increase in d_x, so η increases.

VI. CONCLUSION

We have studied optimal snake motions on an inclined plane. We used a two-dimensional model and determined the effects of the parameters, the transverse and tangential coefficients of friction and the incline angle, on the optimal amplitudes of triangular wave motions and sinusoidal wave motions. When the transverse friction coefficient is much larger than the tangential friction coefficient, we showed that for a given incline angle α and tangential friction coefficient μ_f, the cost of locomotion tends to $(\mu_f\cos\alpha+\sin\alpha)$, with the optimal amplitude scaling as $\mu_t^{-1/4}$. Our analysis also showed a nonmonotonic relationship between the cost of locomotion and the incline angle. The least efficient optimal motion is achieved at a critical incline angle depending on the value of μ_f. The optimal amplitude increases with the incline angle to maintain the upward motion of the snake. For given μ_t and α, the motion becomes less efficient as μ_f increases due to the extra work against tangential friction. However, when μ_f is small, we find that motion with a larger amplitude is more efficient, while when μ_f is large, a motion with smaller amplitude is optimal. We gave an asymptotic analysis of a more general class of motions, and our asymptotic results showed the same scaling laws for optimal amplitude and cost of locomotion.

An extension of this work is to three-dimensional motions of snakes and wider parameter spaces with small or moderate transverse friction coefficients. Another interesting topic is motions in the presence of walls [5,15,16].

ACKNOWLEDGMENTS

We acknowledge helpful discussions on snake physiology and mechanics with David Hu and Hamidreza Marvi, helpful discussions with Fangxu Jing during our previous study of two- and three-link snakes, and the support of NSF-DMS Mathematical Biology Grant No. 1329726, a Sloan Research Fellowship to S.A., and the NSF REU program at the University of Michigan. We thank the anonymous reviewers for their comments.

[1] J. Gray and H. W. Lissmann, J. Exp. Biol. **26**, 354 (1950).

[2] S. Hirose, *Biologically Inspired Robots: Snake-like Locomotors and Manipulators* (Oxford University Press, Oxford, 1993).

[3] H. Astley and B. Jayne, J. Exp. Biol. **210**, 3862 (2007).

[4] D. Hu, J. Nirody, T. Scott, and M. Shelley, Proc. Natl. Acad. Sci. USA **106**, 10081 (2009).

[5] T. Maneewarn and B. Maneechai, in *IEEE International Conference on Robotics and Biomimetics, 2008: ROBIO 2008* (IEEE Press, Piscataway, NJ, 2009), p. 1.

[6] M. Dickinson, C. Farley, R. Full, M. Koehl, R. Kram, and S. Lehman, Science **288**, 100 (2000).

[7] B. C. Jayne, Copeia, **4**, 915 (1986).

[8] R. Shine, H. Cogger, R. Reed, S. Shetty, and X. Bonnet, J. Zool. **259**, 261 (2003).

[9] J. J. Socha, Nature (London) **418**, 603 (2002).

[10] A. Transeth, K. Pettersen, and P. Liljebäck, Robotica **27**, 999 (2009).

[11] K. Pettersen, Ø. Stavdahl, and J. Gravdahl, *Snake Robots: Modelling, Mechatronics, and Control* (Springer, Berlin, 2013).

[12] I. Erkmen, A. Erkmen, F. Matsuno, R. Chatterjee, and T. Kamegawa, IEEE Rob. Autom. Mag. **9**, 17 (2002).

[13] M. Yim, K. Roufas, D. Duff, Y. Zhang, C. Eldershaw, and S. Homans, Auton. Robots **14**, 225 (2003).

[14] R. L. Hatton and H. Choset, in *2010 IEEE International Conference on Robotics and Automation (ICRA)* (IEEE Press, Piscataway, NJ, 2010), p. 691.

[15] H. Marvi and D. Hu, J. R. Soc. Interface **9**, 3067 (2012).

[16] A. Transeth, R. I. Leine, C. Glocker, K. Pettersen, and P. Liljeback, IEEE Trans. Rob. **24**, 88 (2008).

[17] L. Becker, S. Koehler, and H. Stone, J. Fluid Mech. **490**, 15 (2003).

[18] D. Crowdy, S. Lee, O. Samson, E. Lauga, and A. E. Hosoi, J. Fluid Mech. **681**, 24 (2011).

[19] D. Tam and A. E. Hosoi, Phys. Rev. Lett. **98**, 068105 (2007).

[20] J. E. Avron, O. Gat, and O. Kenneth, Phys. Rev. Lett. **93**, 186001 (2004).

[21] J. Lighthill, *Mathematical Biofluiddynamics* (Society for Industrial and Applied Mathematics, Philadelphia, 1975).

[22] J. A. Sparenberg, *Hydrodynamic Propulsion and Its Optimization: Analytic Theory*, Fluid Mechanics and Its Applications Vol. 27 (Springer, Berlin, 1994).

[23] S. Michelin and S. G. Llewellyn Smith, Phys. Fluids **21**, 071902 (2009).

[24] D. Hu and M. Shelley, in *Natural Locomotion in Fluids and on Surfaces* (Springer, New York, 2012), p. 117.

[25] F. Jing and S. Alben, Phys. Rev. E **87**, 022711 (2013).

[26] S. Alben, Proc. R. Soc. A **469**, 20130236 (2013).

[27] R. L. Hatton, Y. Ding, H. Choset, and D. I. Goldman, Phys. Rev. Lett. **110**, 078101 (2013).

[28] Y. Ding, S. Sharpe, A. Masse, and D. Goldman, PLoS Comput. Biol. **8**, e1002810 (2012).

[29] S. Hirose and H. Yamada, IEEE Rob. Autom. Mag. **16**, 88 (2009).

[30] J. Nocedal and S. J. Wright, *Numerical optimization* (Springer-Verlag, Berlin, 1999).